Catal Lett (2008) 120:71–81
DOI 10.1007/s10562-007-9251-1

A Comparative Study on the Catalytic Activity of Mn Containing MCM-41 Molecular Sieves for Oxidation of *p*-Cymene

S. Vetrivel · A. Pandurangan

Received: 17 March 2007 / Accepted: 23 August 2007 / Published online: 11 September 2007

Abstract Mesoporous silica molecular sieves SiMCM-41, AlMCM-41 with Si/Al ratio equal to 158 and MnMCM-41 with Si/Mn ratio equal to 29 were synthesized by hydrothermal method. Manganese oxide impregnated on SiMCM-41 and on AlMCM-41 catalysts were also prepared by wet impregnation method. These catalysts referred as Mn/SiMCM-41 and Mn/AlMCM-41 (158). Both the manganese incorporated and impregnated catalysts structure was elucidated by XRD. Nitrogen adsorption isotherm was used to determine specific surface area, pore volume, and pore size distribution. The thermal stability of the as-synthesized catalyst was studied using TG-DTA. The presence of Mn^{2+} was evident through DR UV–VIS and ESR spectroscopy. Through ESR studies, MnMCM-41 (29) was assigned to have framework Mn(II) sites. Extra-framework manganese species with well-resolved sextet, centered at g = 2.00 had octahedral symmetry was observed in Mn/SiMCM-41 and Mn/AlMCM-41 (158). Mn retained its +2 oxidation state (ESR active) even upon calcination at 550 °C in presence of air. The catalytic activity of the above-mentioned manganese containing MCM-41 catalysts were tested by vapor phase oxidation of *p*-cymene with CO_2-free air in the temperature range from 200 to 400 °C in steps of 50 °C. The major products were 4-methylacetophenone (4-MAP), 4-isopropyl benzaldehyde (4-IPB), 1,2-epoxyisopropyl benzaldehyde or 1,2-epoxycumenaldehyde (1,2-ECA) and 4-methyl styrene (4-MS). Among the product selectivity, (4-MAP) was found to be higher than that of others. The order of the activity of catalysts followed Mn/SiMCM-41 > Mn/AlMCM-41 (158) > MnMCM-41 (29) > Mn/SiO_2.

Keywords MCM-41 · Oxidation · *p*-Cymene · 4-Methylacetophenone · 4-Isopropyl benzaldehyde

S. Vetrivel (✉)
Department of Chemical Engineering, National Taiwan University of Science and Technology, Taipei 106, Taiwan ROC
e-mail: svetrivel05@yahoo.co.in

S. Vetrivel · A. Pandurangan
Department of Chemistry, Anna University, Chennai 600 025, India

1 Introduction

The selective oxidation of organic substrates using dioxygen (molecular oxygen) as the ultimate oxidant is a very important synthetic and industrial goal. With respect to its use in the manufacture of organic chemicals, catalytic oxidation with dioxygen traditionally holds a very prominent place in the petrochemical industry, where, it is by far the most important technology for the upgrading of hydrocarbons [1]. One of the reasons for the necessity of catalytic oxyfunctionalization is due to rather forcing reaction conditions (high temperature and pressure) required for traditional oxidation with dioxygen [2]. Oxidation of *p*-cymene is an industrially important reaction, because of its 4-methylacetophenone product, which is used as a precursor for manufacture of perfumes and the other product of this reaction is 4-isopropylbenzaldehyde, which is also used as a flavoring agent for food materials [3]. Oxidation of *p*-cymene with manganese (III) porphyrin complex catalysts in the presence of hydrogen peroxide as the oxidant, using co-catalysts, like imidazole or ammonium acetate is already reported [4, 5]. In spite of the excellent performance of this catalyst, there are some drawbacks. For instance, the co-catalyst is used to facilitate the desired heterocylic cleavage of H_2O_2 and to stabilize the porphyrin Mn(V) = 0 complex formed in the oxidation

cycle [6]. Aleksandrov [7] and Basaeva et al. [8] reported the same reaction catalysed by Co and Mn complexes in acetic acid medium. Cerium (IV) ammonium nitrate in acetic acid to give nitro and acetate substituted derivatives [9] and oxides of Cr, Mn and Se have also been reported [10]. For the production of 4-isopropylbenzaldehyde, Vaudano and Tissot [11] carried out the reaction in methanolic medium by direct electrochemical oxidation method. Oxidation of *p*-methyltoluene and *p-tert*-butyltoluene catalysed by Co, Mn and NaBr salts in acetic acid medium and vapour phase oxidation of *p*-methoxy toluene over vanadium pentoxide based catalysts have also been reported [12–18]. Recently Kala Nair et al. [3] reported the aerial oxidation of substituted aromatic hydrocarbons catalysed by $Co/Mn/Br^-$ in water-dioxygen medium in the temperature range 383–423 K, in which, the *p*-isopropylbenzyl alcohol (54.7%) selectivity was more predominant than other products in the oxidation of *p*-cymene. In the present study the oxidation of *p*-cymene on manganese-containing mesoporous MCM-41 molecular sieves was carried out at high temperature. Many research groups worked on the immobilization of Mn complexes onto the mesoporous material. Burch et al. [19] prepared surface-grafted manganese-oxo species on the walls of MCM-41 channels. Caps and Tsang [20] prepared Mn-MCM-41 with a molecular organic chemical vapor deposition (MOCVD) method. Yonemitsu et al. [21] firstly developed the template ion-exchange (TIE) method for the synthesis of Mn-MCM-41, and they argued that manganese was highly dispersed in the mesopore of MCM-41 and only existed as Mn^{2+}. Based on their results, in the present study, the synthesis of manganese-containing MCM-41 catalysts, their physicochemical characterization and application as catalysts for the oxidation of *p*-cymene was investigated. Owing to its less cost, and extensive use in industries, air was chosen as an oxidant instead of hydrogen peroxide and tertiary butylhydrogen peroxide.

2 Experimental

2.1 Hydrothermal Synthesis of MCM-41 Materials

The AlMCM-41 (Si/Al = 158) was synthesized hydrothermally using a gel composition of $1SiO_2$:$0.007Al_2O_3$:$0.2CTAB$:$0.89H_2SO_4$:$120H_2O$. Sodium metasilicate and aluminium sulfate were used as the sources for silicon and aluminium, respectively. Cetyltrimethylammonium bromide (CTAB) was used as the structure-directing agent. In a typical synthesis, 21.2 g of sodium metasilicate dissolved in deionized water was combined with 0.45 g of aluminium sulfate in deionized water. The pH of the solution was adjusted to 10.5 with constant stirring up to form a gel. After that 7.3 g of cetyltrimethylammonium bromide was added to it and the stirring was continued for 3 h at room temperature so that the gel was changed into suspension. The suspension was transferred into a Teflon-lined steel autoclave, sealed and heated in air oven at 160 °C for 48 h. After cooling to room temperature, the product formed was filtered, washed with deionized water, dried and finally calcined in flowing air at 550 °C for 6 h.

The catalyst SiMCM-41 was synthesized in an above similar manner without aluminium sulfate and the input gel molar composition was $1SiO_2$:$0.2CTAB$:$0.89H_2SO_4$:$120H_2O$. The MnMCM-41 catalyst (Si/Mn = 29) was also synthesized using above procedure wherein, only the change of manganese(II) acetate was adjusted appropriately and the input gel molar composition was $1SiO_2$:$0.04MnO$:$0.2CTAB$:$0.89H_2SO_4$:$120H_2O$.

2.2 Preparation of Manganese Impregnated Catalysts

About 0.3 M manganese(II) acetate solution was prepared and mixed with 3 g of SiMCM-41 or AlMCM-41 under constant stirring. The solution was dried under reduced pressure, and calcined in air at 550 °C for 6 h. The freshly silica supported manganese oxide catalyst was synthesized according to the previous reports [22].

2.3 Physicochemical Characterization

The manganese content in hydrothermally synthesized MnMCM-41 (29) and the aluminium content of AlMCM-41 (158) was determined using ICP-AES with allied analytical ICAP 9000. XRD analysis was performed on a Scintag 2000 diffractometer equipped with liquid nitrogen-cooled germanium solid-state detector using CuKα radiation. The samples were scanned between 0.5° and 10° (2θ) in steps of 0.02 with the counting time of 5 s at each point. ASAP-2010 volumetric adsorption analyzer manufactured by the Micromeritics Corporation (Norcross, GA) was used to determine the specific surface area of the materials at liquid nitrogen temperature. Before the measurement, each sample was degassed at 623 K at 10^{-5} torr overnight in an out gassing station of the adsorption apparatus. The full adsorption–desorption isotherm was obtained using BET method at various relative pressures; the pore size distribution and wall thickness were calculated from the nitrogen adsorption–desorption isotherms using the BJH algorithm (ASAP 2010 built in software from Micromeritics). Thermal decomposition of the as-synthesized samples was examined on Rheometric scientific (STA 15 H^+) thermo balance. About 10–15 mg of as-synthesized MCM-41 sample was placed in a platinum pan and heated from room temperature to 1,000 °C at a heating rate 20 K min^{-1} in air with a flow rate

of 50 mL min^{-1}. The co-ordination environment of Mn-containing MCM-41 samples was examined by diffuse reflectance UV–VIS spectroscopy. The spectra were recorded between 200 and 800 nm on a Shimadzu (UV–VIS Spectrophotometer Model 2101 PC) using $BaSO_4$ as the reference and Ocean Optics (Fibler Optics Spectrometer Model Inc. SD 2000) with charged coupled device detector using MgO as reference. The manganese environment was analyzed by ESR technique (Varian E112 spectrometer operating in the X-band 9-GHz region). DPPH was used as the reference to mark the 'g' value. The relative ESR intensities were calculated by double integration of the recorded ESR signal. The morphology of MCM-41 samples was recorded using a JEOL 640 scanning electron microscope operating at an accelerating voltage of 10 kV. Samples were mounted using a conductive carbon double-sided sticky tape. The samples were sputtered with gold (ca. 10 nm) to reduce the effect of charging.

2.4 Catalytic Reaction—Oxidation of *p*-Cymene

The catalytic activity manganese containing catalysts were carried out in an ordinary fixed bed continuous down flow quartz reactor under atmospheric pressure in the temperature range of 200–400 °C in steps of 50 °C. About 0.3 g of catalyst was mixed with porcelain beads (3 mm diameter) vertically loaded in the center of a vertical bed reactor, with glass wool being packed above and below the catalyst bed. The reactor was placed coaxially in the cylindrical ceramic tube furnace of internal diameter 3.5 cm, coated with a thin layer of asbestos and wound uniformly with Nichrome wire. The furnace temperature was raised to the requisite level by adjusting the controller. When the reaction temperature attained a constant value, the syringe was filled with the *p*-cymene and attached to the duel syringe pump. The liquid reactant was injected into the reactor containing the catalyst bed by a microdisplacement pump. The product mixture was collected for a time interval of 1 h. The weight percentage conversion of *p*-cymene was analysed by gas chromatograph (Hewlett-Packard 5890) with an FID type detector equipped with PONA capillary column (50 m length and 0.21 mm o.d., coated with a 0.5 mm thick film of stationary phase). The identification of products was performed on a Shimadzu GC-MS-QP1000EX gas chromatograph-mass spectrometer. All the catalysts were regenerated by burning away the coke deposit by passing air at a temperature of 500 °C for 6 h.

3 Results and Discussion

3.1 Elemental Analysis

The aluminium and manganese ions content in hydrothermally synthesized AlMCM-41 (158) and MnMCM-41 (29) have been observed using ICP-AES. From the ICP-AES analysis, aluminium content in AlMCM-41 (158) was found to be 0.052 g and manganese content in MnMCM-41 (29) was found to be 0.155 g, respectively.

3.2 X-ray Diffraction

The powder XRD patterns of calcined SiMCM-41, AlMCM-41 (158) and MnMCM-41 (29) catalysts are shown in Fig. 1. It can be observed that all the above materials exhibit a strong peak in the 2θ range of 1.9–2.4°. Additionally, the broad peaks at 2θ range of 3.5–4.6° indicating the formation of well-ordered mesoporous materials. The d_{100} values and unit cell parameters of the calcined materials are listed in Table 1. The differences in intensity of the reflections are not highly significant: Marler et al. [23] have shown that the intensities of the X-ray diffraction peaks are related to the difference in scattering power between the amorphous silica wall and the in-pore amorphous organic phase. The hexagonal unit cell parameter (a_o) was calculated using the formula $a_o = 2d_{100}/\sqrt{3}$, which was obtained from the peak in the XRD pattern by Bragg's equation ($2d \sin\theta = \lambda$, where $\lambda = 1.54$ Å for the CuKα radiation). The value of a_o is equal to the internal pore diameter plus one pore wall thickness [24]. Further, the appearance of the above peaks in manganese and aluminium incorporated MCM-41 catalysts suggested that the hexagonal array of mesopores in MCM-41 was sustained after the incorporation of metal in the framework. The higher *d*-spacing and unit cell parameter values observed

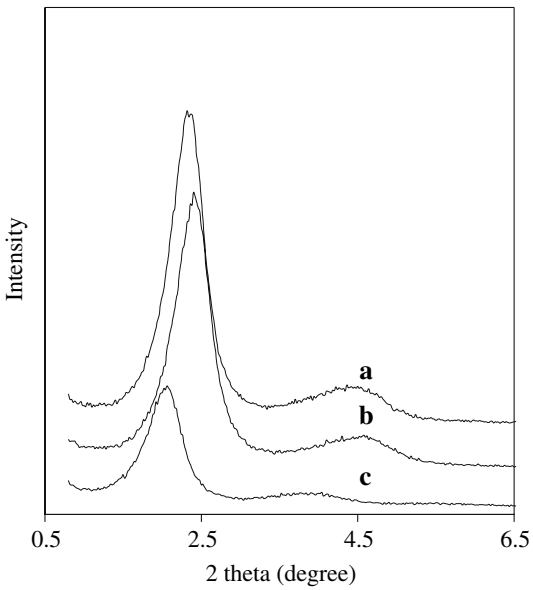

Fig. 1 XRD spectra of calcined (a) SiMCM-41, (b) AlMCM-41 (158) and (c) MnMCM-41 (29)

Table 1 Physicochemical characterization of MCM-41 type materials

Catalysts	*d*-spacing[a] (Å)	Unit-cell parameter[a] (Å)	Surface area[b] ($m^2\ g^{-1}$)	Pore size[b] D (Å)	Pore volume[b] (cm^3/g)	Wall thickness[b] (Å)
SiMCM-41	36.21	41.81	1041	33.9	0.99	10.07
AlMCM-41 (158)	37.44	43.23	949	30.1	0.95	16.27
MnMCM-41 (29)	41.68	48.13	894	28.0	0.75	22.01

[a] Values obtained form XRD studies

[b] Values obtained form N_2-adsorption results

for MnMCM-41 (29) suggest an incorporation of metal in the framework locations [25] because its (Mn–O (∼1.7308)) longer bonding length than Si–O (∼1.509). However, there is no regular rule in MCM-41 as it has an amorphous structure where both bond length and angle may be change. Further, during calcination, the 100 reflection shift to higher value indicating a contraction of the lattice caused by template removal and subsequent condensation of silanol groups, which has been reported for MCM-41 [26]. The decrease in XRD signal intensity after calcination of MCM-41 is due to the saturation of the materials with air.

3.3 Nitrogen Adsorption–Desorption Isotherm Analysis

The nitrogen adsorption–desorption isotherms of the calcined SiMCM-41, AlMCM-41 (158) and MnMCM-41 (29) samples exhibited the sharp characteristic of mesoporous materials with regular pore size. The adsorption–desorption isotherms of these catalysts are presented in Fig. 2a. It is observed that there are three distinct well-defined stages in the isotherm. The monolayer adsorption on the walls of the mesopores is responsible for the nitrogen uptake at low relative pressures ($P/P_o < 0.3$). A sharp steep at intermediate P/P_o may indicate the capillary condensation in the mesopores and a plateau portion at high P/P_o associated with multilayer adsorption on the external surface of the materials. All the catalysts show a characteristic step around $P/P_o \approx 0.3$ indicating the mesoporous nature of the materials [27]. The sharpness and height of the capillary condensation step are the indications of pore size uniformity. Deviations from sharp and well-defined pore filling step are the indication of increase in pore size heterogeneity. From the plot of the pore-size distribution, we can see a well-defined pore size distribution centered around 30 Å. The pore size distribution curves of the metal containing MCM-41 show a slight decrease in their half-height width of the peak at around 30 Å, compared with that of the SiMCM-41 sample (figure not given). It indicates that the mesoporosity was somewhat degraded after incorporation of the metal. The pore size distribution of these mesoporous materials, their corresponding BET surface area and the pore volumes are listed in Table 1. It indicates that the metal containing samples have thicker pore walls and lower surface area than the siliceous MCM-41.

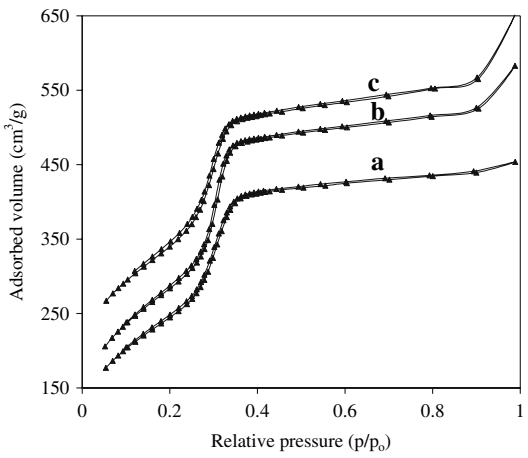

Fig. 2 N_2-adsorption isotherm of calcined (a) SiMCM-41, (b) AlMCM-41 (158) and (c) MnMCM-41 (29)

3.4 TG-DTA Study

Thermogravimetric and differential thermal analysis of the SiMCM-41, AlMCM-41 (158) and MnMCM-41 (29) catalysts are given in Fig. 3. The thermal patterns of the three samples are qualitatively very similar. The TGA patterns have at least three distinct stages of weight losses that depend on framework composition. A first weight loss ∼4.19–11.61% was observed between 50 and 150 °C corresponds to desorption and removal of the water molecules physisorbed on the external surface of the crystallites or occluded in the macropores and mesopores present between the crystallite aggregates. The second stage of 150–350°C, corresponding to a weight loss ∼15.16–29.47% can be ascribed to the decomposition of the surfactant species. Finally, the weight loss ∼5.41–11.47% from 350 to 550 °C can be assigned to water loss from the condensation of adjacent silanol groups to form a siloxane bond. The total

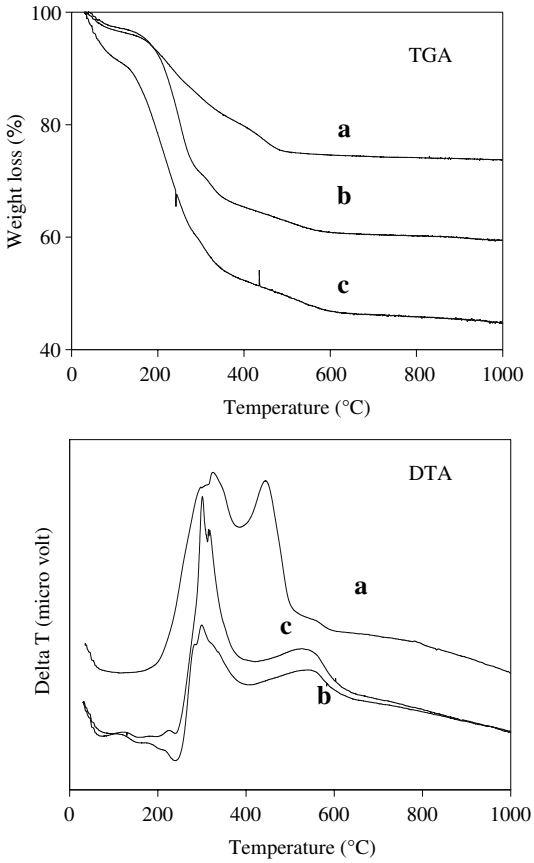

Fig. 3 TGA curve of as-synthesized (a) MnMCM-41 (29), (b) SiMCM-41 and (c) AlMCM-41 (158)

weight losses are 37.80, 52.57 and 24.76 wt% for samples SiMCM-41, AlMCM-41 (158) and MnMCM-41 (29), respectively. The weight loss was higher in AlMCM-41 (158) than SiMCM-41 and MnMCM-41 (29).

Thermogravimetric analysis in combination with XRD peaks showed that samples were thermally stable at calcination conditions. The organic template was decomposed below 550 °C, the weight loss for all of the samples was in the range of about 10–53 wt%, which indicated that as-synthesized samples contained large amounts of organic templates because of the presence of mesoporous materials with large void volume [28]. The DTA curves are shown in the Fig. 3. All the curves in the broad exotherm between 200 and 550 °C coincide with the weight loss in the TGA traces between 200 and 550 °C. Hence, it is ascribed to the loss of oxidative decomposition of template. Above 550 °C, there is neither exothermic nor endothermic peak illustrating the materials are stable.

3.5 DR UV–VIS Spectroscopy

The calcined MnMCM-41 (29), Mn/SiMCM-41 and Mn/AlMCM-41 (158) samples were characterized by diffuse reflectance UV–VIS spectroscopy between 200 and 800 nm. The plot of wavelength versus reflectance is shown in Fig. 4. Two bands at 270 and 500 nm were observed for these samples except MnMCM-41 (29). The charge transfer transition of $O^{2-} \rightarrow Mn^{2+}$ in Mn_3O_4 in which Mn was disordered octahedrally coordinated with oxygen exhibited a band at 320 nm [29]. We thus tentatively assigned the intense band observed at lower wavelength at 270 nm to the charge transfer transition of $O^{2-} \rightarrow Mn^{3+}$ in tetrahedral coordination. The $A_{1g} \rightarrow T_{2g}$ crystal filed transitions of Mn^{2+} in Mn_2O_3 or MnO showed a band at 500 nm [29]. Thus the band at 500 nm was assigned to Mn^{2+} probably existing on the surface of MCM-41. These absorption maxima coincide with the reports in the literature [30]. From the above results, it is inferred that the Mn^{2+} and Mn^{3+} ions may be coordinated with Si(IV) by disordered octahedral and tetrahedral environments, respectively. In the case of Mn/SiMCM-41 and Mn/AlMCM-41 (158) samples, as Mn is in the non-framework it is to have in octahedral environment of oxygen [31]. As Mn in +2 oxidation state, proved by ESR spectroscopy. It is to have ^6S groundterm. As ^6S does not have crystal field componance. The electronic excitations are forbidden, but there may spin orbit interactions, as reported in the literature [32] with which some transitions may have allowance. In conformation of this in the DR UV spectra that the Mn/SiMCM-41 and Mn-AlMCM-41 (158) those absorption band are absorbed. But they cannot be due to $^6A_{1g} \rightarrow {}^4T_{2g}$ and charge transfer transition as reported in the literature [29, 33].

3.6 ESR Spectroscopy

Figure 5 shows the X-band ESR spectra of manganese containing MCM-41 at liquid nitrogen temperature. The ESR spectra of MnMCM-41 (29) display five signals characteristics of Mn^{2+} ($3d^5$) species. Low intensity forbidden transitions are evident that the Mn^{2+} ions are rather incorporated. Iwamoto and coworkers [21] found a typical Mn^{2+} ESR signal for the Mn-MCM-41 (Si/Mn = 20, TIE) and suggest that manganese existed as Mn^{2+} in their TIE sample. We attribute the absence of ESR signal in the Mn^{3+} species. Since Mn^{3+} is more inclined than Mn^{2+} to be substituted for Si^{4+} at the framework position of zeolites or MCM-41. Mn^{3+}, which would have been formed during synthesis, is observed to be at least part of the Mn^{3+} reduced to Mn^{2+} during calcination [34]. In the as-synthesized Mn-containing aluminophosphate molecular sieves, synthesized under acidic condition, spectra similar to this were also reported [35]. The Mn^{2+} substituted MCM-41 molecular sieves show a broad ESR signal with a g value 2.007. From the above results, it is inferred that the

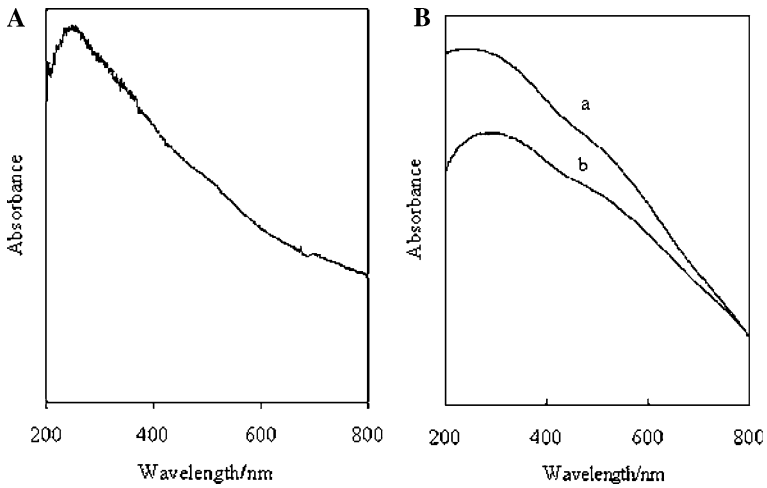

Fig. 4 DR UV–VIS spectra of (**A**) calcined MnMCM-41 (29), (**B**) calcined (a) Mn/SiMCM-41, (b) Mn/AlMCM-41 (158)

Mn^{2+} is coordination to Si(IV) by distorted octahedral environment.

The amount of incorporation of extra-framework Mn(II) ions into Mn/SiMCM-41 and Mn/AlMCM-41 (158) is shown in Fig. 5a and b. There are six hyperfine lines centered at g = 2.00 corresponding to Mn^{2+} in octahedral environment. Similar observations were also noted for Mn-MCM-41 [36] and MnAlPO-5 [35] with the manganese species located at extra-framework positions. In the ESR spectrum, the splitting of the sextet increases from 3,010 to 3,550 G. Meanwhile, the peak-to-peak line-width increases and the line height decreases. These observations indicate that the Mn^{2+} ions strongly interact with their environment in the octahedral coordination, which is consistent with an extra-framework position [37].

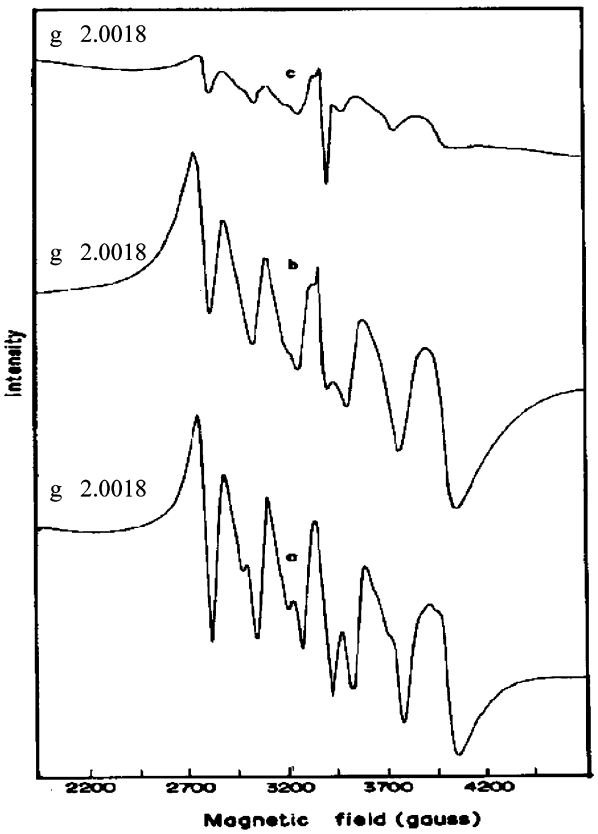

Fig. 5 ESR spectra of calcined (a) Mn/SiMCM-41, (b) Mn/AlMCM-41 (158) and (c) MnMCM-41 (29)

3.7 SEM Analysis

The morphology and the long-range order of AlMCM-41 (158), MnMCM-41 (29), Mn/SiMCM-41 and Mn/AlMCM-41 (158) were investigated by scanning electron microscopy. The SEM pictures of these catalysts are presented in Fig. 6. The pictures show the orderly growth of pure hexagonal phase with well-defined sites. Because all materials have been synthesized using cetyltrimethylammonium bromide as surfactant in liquid crystal template mechanism, Steel et al. [38] postulated that CTMABr surfactant molecules assembled directly into the hexagonal liquid crystal phase upon addition of the silicate species. In the case of manganese impregnated catalysts (Fig. 6c and d), it can be seen that, irrespective of the manganese loading, the solids have the same morphology which corresponds to aggregates without regular shapes.

3.8 Influence of Temperature

The variation of reaction temperature on vapour phase oxidation of *p*-cymene was carried out over Mn/SiMCM-41, Mn/AlMCM-41 (158), MnMCM-41 (29) and Mn/SiO_2 at 200, 250, 300, 350 and 400 °C. The flow rate of *p*-cymene was 1 mL h^{-1} and that of air was 50 mL min^{-1}. The major products 4-methylacetophenone (4-MAP), 4-isopropylbenzaldehyde (4-IPB), 1,2-epoxyisopropyl benzaldehyde or 1,2-epoxycuminaldehyde (1,2-ECA) and 4-methylstyrene

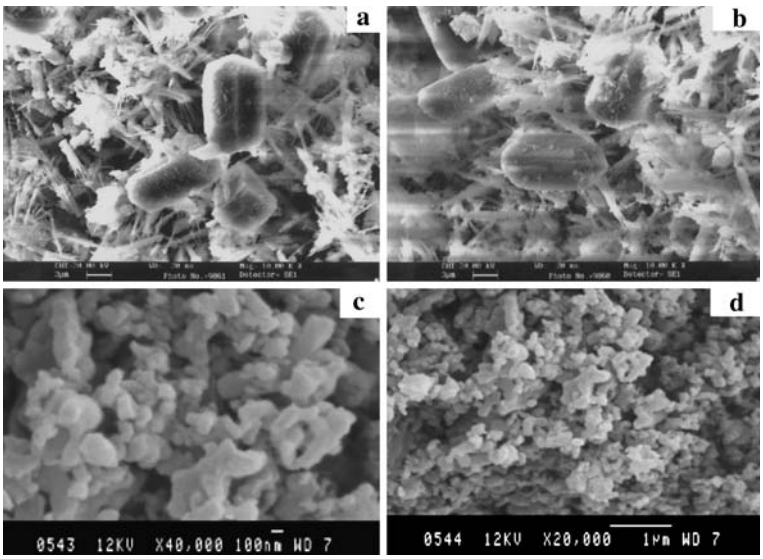

Fig. 6 SEM picture have (a) AlMCM-41 (158), (b) MnMCM-41 (29), (c) Mn/SiMCM-41 and (d) Mn/AlMCM-41 (158)

(4-MS). The *p*-cymene conversion and product selectivity are presented in the Table 2. It is clearly indicated that the conversion increased steadily with increasing reaction temperature up to 350 °C, but at 400 °C it decreased. The decrease at the latter temperature is due to coke formation. Based on the products formed in this reaction, it is supposed that most of the manganese would be in the octahedral coordination formed by tiny particles of manganese oxide which are to rest in the channel surface of MCM-41. Among the product selectivity, 4-MAP was observed as a major product whose selectivity increased with increase in temperature up to 350 °C, but decreased at 400 °C. Mn/SiMCM-41 shows maximum 4-MAP selectivity (61.2%) at 350°C than other catalysts. In the case of Mn/AlMCM-41 (158) catalysts, the selectivity to 4-MAP was 55.3%, which is considerably lower than that observed over Mn/SiMCM-41. Formation of 4-MAP can be understood based on the reaction Scheme 1.

Initially Mn(II) in the non-framework may be oxidized to Mn(IV) by oxygen [39]. There might be a simultaneous

Table 2 Products distribution of *p*-cymene oxidation over different catalysts at different reaction temperature

Catalysts	Temperature (°C)	Conversion (wt%)	Selectivity (%)				
			4-MAP	4-IPB	1,2-ECA	4-MS	Others
Mn/SiMCM-41	200	43.8	37.6	5.8	6.8	42.3	7.5
	250	46.2	44.6	7.1	8.5	32.1	7.7
	300	55.2	52.8	10.0	11.5	15.4	10.3
	350	62.7	61.2	15.3	13.8	8.1	1.6
	400	51.5	55.3	26.4	15.3	2.1	0.9
Mn/AlMCM-41 (158)	200	37.6	36.4	8.0	8.1	40.3	7.2
	250	41.9	43.4	10.3	10.0	30.0	6.3
	300	47.9	49.0	14.4	14.0	15.1	7.5
	350	51.7	55.3	19.8	15.2	7.6	2.1
	400	43.1	48.0	31.3	17.6	3.1	–
MnMCM-41 (29)	200	36.7	35.7	12.5	10.5	38.5	2.8
	250	39.0	41.8	15.6	13.4	26.4	2.8
	300	45.1	47.6	17.5	17.5	13.9	3.5
	350	48.8	50.3	22.0	18.5	6.2	3.0
	400	43.0	45.7	33.1	20.1	1.1	–
Mn/SiO_2	200	10.9	4.0	1.8	–	76.8	17.4
	250	21.9	7.2	3.6	2.2	73.9	13.1
	300	24.8	7.6	4.7	3.2	69.4	15.1
	350	32.1	8.3	6.5	5.5	61.3	18.4
	400	18.6	6.1	8.4	6.3	59.4	19.8

Reaction condition: 0.3 g of catalyst; flow rates: 1 mL/h for reactants and 50 mL/h for air

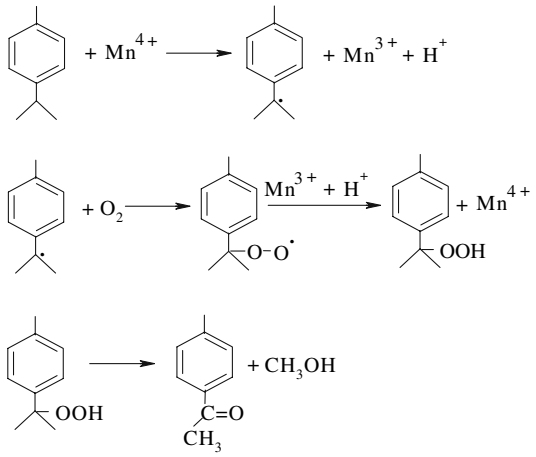

Scheme 1

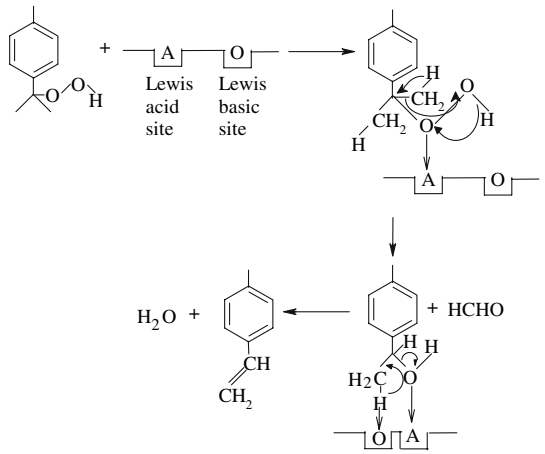

Scheme 2

electron transfer to manganese and proton release from the tertiary hydrogen of *p*-cymene. The resulting free radical combines with oxygen to form superoxide. This superoxide abstracts a tertiary hydrogen atom from other *p*-cymene to yield hydroperoxide. This hydroperoxide decomposes thermally to yield 4-MAP and methanol. In another possibility, the superoxide may be converted to hydroperoxide by picking up an electron from Mn^{3+}, and combining with the already released H^+ as shown in the reaction Scheme 1. This route seems to be more appropriate than the previous one, as the role of Mn^{4+} is retained. The selectivity of 4-MAP which, increased from 200 to 350 °C, may be explained as follows. Since, the decomposition of hydroperoxide is suggested to occur thermally, its formation alone is important. Therefore the decrease at 400 °C might be attributed to partial blocking of active sites by coke.

The selectivity to 4-MS decreased with increase in temperature over all the catalysts. Among the manganese impregnated catalysts, the Mn/SiMCM-41 shows higher 4-MS selectivity than other manganese containing MCM-41 at all temperature studied. The formation of 4-MS can be explained by the reaction Scheme 2.

The hydroperoxide which decomposes thermally to give 4-MAP, can also be decomposed to yield 4-MS through complexation with the Lewis acid sites of the metal oxide particles. The hydroperoxide co-ordinates to the Lewis acid sites through oxygen adjacent to the alkyl group. This co-ordination activates the adjacent oxygen. This activated oxygen is added to one of the methyl groups in order to yield formaldehyde. The reorganisation of atoms and bonds is illustrated clearly in the Scheme 2. Once formaldehyde is released, the resulting alcohol derivative undergoes dehydration over the same metal oxide particle to yield 4-MS. As the alcohol derivative is not observed in this reaction, either it must form freely and decompose instantaneously to give 4-MS or may not be freely formed, so that the whole process of formation of formaldehyde and dehydration of 4-MS may be a single step process. The decrease in the selectivity of 4-MS with increase in temperature can be due to the decreased co-ordinated interaction of hydroperoxide with Lewis acid sites of the metal oxide particles.

The selectivity to 4-IPB increased from 200 to 400 °C over all the catalytic systems studied. The formation of 4-IPB is explained in the reaction Scheme 3. There is Mn^{4+} that abstract electron from methyl group of *p*-cymene to form free radical. Here, abstraction of electron from methyl group *p*-cymene rather than isopropyl group is considered. The radical is stable, as there is a possibility of resonance. In the previous two reactions (Schemes 1 and 2), the abstraction of electron from the tertiary C–H bond is considered, but here the same from methyl hydrogen is considered. Based on this observation, it is suggested that tiny metal oxide particles can have varying degree of activity, as the size and surface free energy of them are different. The free radical reacts with molecular oxygen to

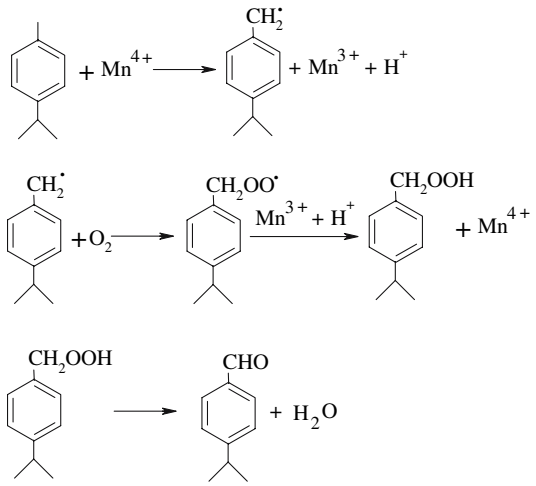

Scheme 3

produce superoxide, which then gets converted to peroxide, similar to reaction Schemes 1 and 2. The thermal decomposition of this peroxide is suggested to yield 4-IPB. Increase in selectivity with increase in temperature might be attributed to requirement of thermal energy for the decomposition of peroxide.

The selectivity to 1,2-ECA increased from 6.8 to 15.3% with increase in temperature over Mn/SiMCM-41. The Mn/AlMCM-41 (158) show similar trend for 1,2-ECA and the values are slightly less than Mn/SiMCM-41. The formation of this product is illustrated in the reaction Scheme 4.

Since, 1,2-ECA is the precursor of the aldehyde, the latter is suggested to react with Mn^{4+} of the metal oxide particles to yield the free radical. The free radical in turn reacts with molecular oxygen to produce superoxide. The latter species is converted to hydroperoxide similar to the previous reaction schemes. The thermal decomposition of hydroperoxide gives the1,2-ECA. A point to note is, though 1,2-ECA was observed in this study, 4-methyl-1,2-epoxyisopropylbenzene is not observed. Either this product would not have been formed in this study or would have remained along with unidentified products. So the selectivity of 1,2-ECA increased with increase in temperature. The increase might be due to high activation energy requirement for abstraction of hydrogen atom from the tertiary carbon. The presence of formyl group in the para position can also contribute to the increase in activation energy, as it is an electron-withdrawing group.

Comparison of activity and selectivity of manganese incorporated catalyst allow us to study the effect of manganese substitution in the framework on conversion and product selectivities. The activity of manganese incorporated MnMCM-41 (29) is always found to be less than that of manganese impregnated catalysts at all the temperatures studied. It shows similar trend for conversion and product selectivity as that of manganese impregnated catalysts. Hence, there may not be any change in the major class of the reactions that occur over this catalyst. Comparison of conversion illustrates slightly less value for this catalyst than the former. This might be due to the more dispersion of manganese oxide particles in non-framework of Mn/SiMCM-41 than in MnMCM-41 (29). The selectivity to 4-MAP increased from 200 to 350 °C, but at 400 °C it decreased. This trend is similar to that observed over Mn/SiMCM-41. The selectivity to 4-IPB, 1,2-ECA and 4-MS also exhibits the same trend as that of Mn/SiMCM-41.

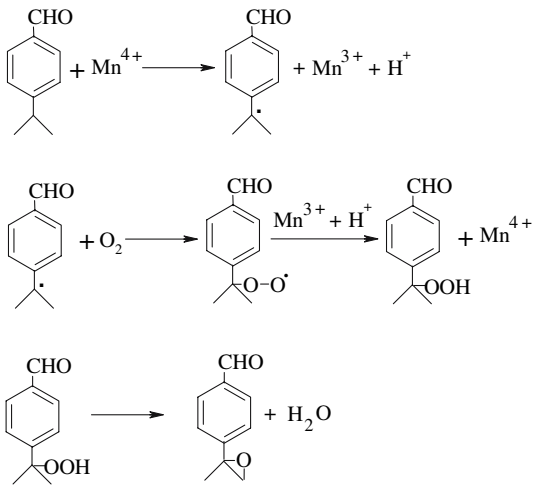

Scheme 4

Further comparison of activities of MCM-41 molecular sieves, the reaction was extended over silica supported manganese oxide catalyst. The results obtained with metal oxide silica mixture, illustrates less conversion but with similar trend. However, selectivity to 4-MS and unidentified products was more, but the selectivity to 4-MAP, 4-IPB and 1,2-ECA is very much less. The very high selectivity to 4-MS clearly illustrates that supporting reaction schemes given above are depending on the particle size of metal oxide. This high selectivity to 4-MS illustrates that the fine particles are more important for the formation of 4-MAP, 4-IPB and 1,2-ECA while the bulkier groups are more suitable for co-ordination assisted activated oxygen insertion to produce formaldehyde and to dehydrate alcohol intermediate to yield 4-MS as illustrated in the reaction Scheme 2.

3.9 Influence of Weight Hourly Space Velocity

The influence of WHSV was tested over Mn/SiMCM-41, Mn/AlMCM-41 (158), MnMCM-41 (29) and Mn/SiO_2 at 3.3, 6.6, 10.3 and 13.3 h^{-1} at 350 °C. The results are illustrated in Table 3. The results show the conversion decreased from 62.7 to 39.0% as the WHSV increased over Mn/SiMCM-41. The selectivity to 4-MAP increased (61.2 to 66.9%) with increase in WHSV. Since *p*-cymene hydroperoxide is the common intermediate to form 4-MAP and 4-MS based on the high selectivity of 4-MAP, it can be said that the decomposition route to 4-MAP would require less activation energy than the other route. In addition, the selectivity to 4-MS decreased with increase in the WHSV. The formation of this product becomes time dependent thus supporting our proposed Scheme 2 involving co-ordination of hydroperoxide on the metal oxide particles to yield 4-MS. The selectivity to 4-IPB increased from 15.3 to 19.0% while the same to 1,2-ECA decreased from 5.0 to 1.1% with increase in WHSV. This observation clearly supports that formation of the latter product depends on the former.

The results of manganese impregnated AlMCM-41 (158) showed lower conversion than Mn/SiMCM-41. The selectivity to 4-MAP increased with increase in WHSV and the values are almost close to Mn/SiMCM-41. This may be

Table 3 Products distribution of *p*-cymene oxidation over different catalysts at different WHSV

Catalysts	WHSV (h^{-1})	Conversion (wt%)	Selectivity (%)				
			4-MAP	4-IPB	1,2-ECA	4-MS	Others
Mn/SiMCM-41	3.3	62.7	61.2	15.3	5.0	15.9	2.6
	6.7	55.2	64.4	16.0	4.4	13.1	2.1
	10.0	48.4	69.1	17.5	2.1	11.3	–
	13.3	39.0	71.8	19.0	1.1	8.1	–
Mn/AlMCM-41 (158)	3.3	51.7	55.3	19.8	8.0	13.6	3.3
	6.7	45.4	60.1	21.1	5.5	10.0	3.3
	10.0	37.3	64.4	23.6	3.8	8.1	0.1
	13.3	34.4	65.9	25.0	2.5	6.6	–
MnMCM-41 (29)	3.3	48.8	50.3	22.0	7.5	15.5	4.7
	6.7	45.1	58.4	23.8	6.2	9.8	1.8
	10.0	36.5	60.6	25.0	4.5	8.0	1.9
	13.3	29.7	63.0	27.5	2.1	7.4	–
Mn/SiO_2	3.3	32.1	8.3	6.5	5.5	61.3	18.4
	6.7	30.1	9.1	7.2	3.7	58.5	21.5
	10.0	29.8	10.8	8.9	2.3	53.1	24.9
	13.3	27.0	13.4	11.2	1.0	49.0	25.4

Reaction condition: 0.3 g of catalyst, temperature 350 °C, and flow rate of air 50 mL/h

due to less amount of manganese content. As observed with the previous catalyst, the selectivity to 4-IPB increased and that of 1,2-ECA and 4-MS decreased with increase in WHSV. The results obtained with manganese incorporated MnMCM-41 (29) catalyst indicated similar trends in conversion and product selectivity as that of Mn/SiMCM-41. But the conversion was slightly less than Mn/SiMCM-41. As said above, it is attributed to the presence of more fine, well dispersed, non-framework manganese oxide in the Mn/SiMCM-41 catalyst. It is also evident based on the less selectivity to 4-MAP. The selectivity to 4-IPB and 1,2-ECA shows similar trend as that of Mn/SiMCM-41.

The results of Mn/SiO_2, illustrates similar trend of decreased conversion with increase in WHSV similar to other catalysts. The selectivity to 4-MAP increased with increase in WHSV, and the selectivity to 4-MS, which was also produced from the hydroperoxide as that of 4-MAP decreased with increase in WHSV. Again 4-MS is to be produced through co-ordination assisted decomposition of *p*-cymene hydroperoxide, which was a time dependent process. The selectivity to 4-IPB increased with increase in WHSV as the formation of 1,2-ECA is again a time dependent process. As the result of this, selectivity to 1,2-ECA decreased with increase in WHSV.

3.10 Influence of Time-on-stream

The effect of time-on-stream on conversion and product selectivity was examined over Mn/SiMCM-41 at 350 °C. The flow rate of *p*-cymene was 1 mL h^{-1} and that of air was 50 mL min^{-1}. This study was carried out for 5 h and it shows fall in catalytic activity and the change in conversion with time. The results are shown in Fig. 7. It clearly depicts the conversion decreased from 62.7 to 45.1% with increase in stream, but the decrease is not much rapid. The selectivity to 4-MAP decreased from 61.2 to 43.9% while that to 4-MS increased from 15.9 to 25.6% with increase in stream. This observation illustrates that co-ordination of *p*-cymene hydroperoxide with manganese facilitates decomposition to 4-MS. Although formation of 4-MAP occurs via thermal degradation of *p*-cumene hydroperoxide, the probability for this hydroperoxide to co-ordinate

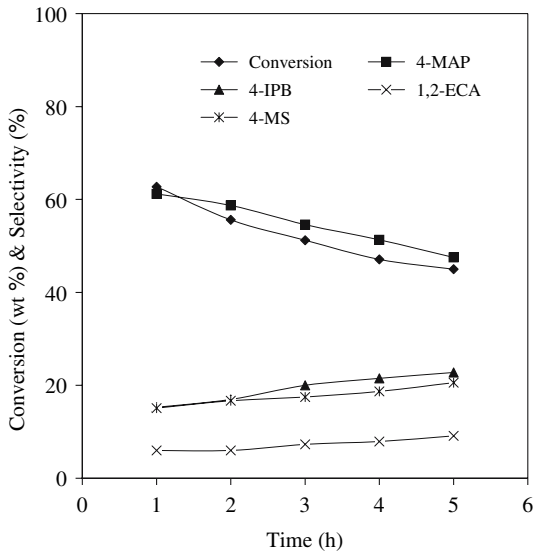

Fig. 7 Effect of time-on-stream on the conversion and product selectivity of *p*-cymene over Mn/SiMCM-41

with manganese is suggested to be highly based on the high selectivity to 4-MS at the latter stage of stream. The selectivity to 4-IPB and 1,2-ECA increased with increase in stream but for the latter increase was not much which was only 9% at the end of 5 h of stream. This observation illustrates the formation of 1,2-ECA on the more active sites.

4 Conclusion

The vapour phase oxidation of *p*-cymene with CO_2-free air over Mn/SiMCM-41, Mn/AlMCM-41 (158), MnMCM-41 (29) and Mn/SiO_2 yields 4-methylacetophenone, 4-isopropyl benzaldehyde, 1,2-epoxy cumenaldehyde and 4-methylstyrene as the major products. Conversion increased from 200 to 350 °C over all the catalysts, but decreased at 400 °C. Finely non-framework fine manganese oxide particles were observed to give high selectivity to 4-methylacetophenone at 350 °C, but bulk particles of Mn/SiO_2 give more selectivity to 4-methylstyrene. Mn/SiMCM-41 is found to be more active than MnMCM-41 (29) catalyst due to its finely dispersed non-framework manganese oxide particles. The formation of 4-methylstyrene through metal co-ordination of *p*-cymene hydroperoxide is suggested in this study. The yield of 4-methylstyrene and 4-methylacetophenone depends on the formation of *p*-cymene hydroperoxide. The formation of 1,2-epoxy cumenaldehyde is shown to be dependent on the yield of 4-isopropyl benzaldehyde. The study of time-on-stream indicates the gradual decrease in conversion with increase in stream. The decrease is attributed to coke formation. Hence, this study illustrates that the MCM-41 supported manganese oxide catalysts are sufficiently active for oxyfunctionalization of *p*-cymene. This study suggests that CO_2-free air can also be a competitive and promising oxidising agent for oxidation of *p*-cymene.

References

1. Fisher RW, Rohrschied F (1996) In: Cornils B, Herrmann WA (eds) Applied homogeneous catalysis with organometalic compounds, vol 1. VCH, Weinheim
2. Wentzel BS, Donners MPJ, Alsters PL, Feiters MC, Nolte RJM (2000) Tetrahedron 56:7797
3. Nair K, Sawant DP, Shanbhag GV, Halligudi SB (2004) Catal Commun 5:9
4. Meunier B (1992) Chem Rev 92:1414
5. Thellend A, Battiom P, Mansuy D (1994) J Chem Soc Chem Commun 1035
6. Hsu YF, Cheng CP (1997) J Mol Catal A: Gen 120:109
7. Aleksandrov VN (1978) Zh Org Khim 14(7):1517
8. Basaeva NN, Obukhova TA, Mironov RP (1976) Osnovn Org Sint Neftekhim 6:11
9. Baciocchi E, Rol C, Ruzziconi R (1984) J Chem Res Synop 10:334
10. Lijuan N, Jinliang J, Zang Y (1997) Jingxi Huagong 14(4):45
11. Vaudano F, Tissot P (2001) Elect Acta 46:875
12. Shimizu N, Saito N, Michio U (1989) Stud Surf Sci Catal 44:131
13. Kristi AF, US Patent US4740614
14. Ger. Offen, DE 3440407
15. Jones GH (1982) J Chem Res (S) 207
16. Barton DHR, Martell AE, Sawyer DT (eds) (1993) The activation of dioxygen and homogeneous catalytic oxidation. Plenum Press, New York
17. Partenheimer W (1991) J Mol Catal 67:35
18. Zaidi SAH (1986) Appl Catal 27:99
19. Burch R, Cruise N, Gleeson D, Tsang SC (1996) J Chem Soc Chem Commun 951
20. Caps V, Tsang SC (2000) Catal Today 61:19
21. Yonemitsu M, Tanaka Y, Iwamoto M (1997) Chem Mater 9:2679
22. De G, Karmakar B, Ganfuli D (2000) J Mater Chem 10:2289
23. Marler B, Oberhagemann U, Vortmann S, Gies H (1997) Micropor Matter 6:375
24. Vetrivel S, Pandurangan A (2004) Appl Catal A: Gen 264:243
25. Luan Z, Xu J, He H, Klinowski J, Kevan L (1996) J Phys Chem 100:19595
26. Kresge CT, Leonowicz ME, Roth WJ, Vartuli JC, Beck JS (1992) Nature 359:710
27. He N, Bao S, Xu Q (1998) Appl Catal A: Gen 169:29
28. Chen YW, Lu YH (1999) Ind Eng Chem Res 38:1893
29. Velu S, Shah N, Jyothi TM, Sivasankar S (1999) Micropor Mesopor Mater 33:61
30. Zhang Q, Wang Y, Itsuki S, Shishido T, Takehira K (2002) J Mol Catal A: Chem 188:189
31. Vetrivel S, Pandurangan A (2005) Ind Eng Chem Res 44:692
32. Cotton FA, Wilkinson G (1966) Advanced inorganic chemistry. Wiley Eastern Private Limited, New Delhi
33. Molella F, Gallardo-Amores JM, Baldi M, Busca G (1998) J Mater Chem 8:2525
34. Vetrivel S, Pandurangan A (2004) J Mol Catal A: Chem 217:165
35. Levi Z, Raitsimring AM, Goldfarb D (1991) J Phys Chem 95:7830
36. Xu J, Luan A, Wasowiscz T, Kevan L (1998) Micropor Mesopor Mater 22:179
37. Zhao DY, Goldfarb D (1995) In: Bonneviot L, Kaliaguine S (eds) Zeolites: a refined tool for designing catalytic sites. Elsevier, Amsterdam, p 181
38. Steel A, Carr SW, Anderson MW (1994) J Chem Soc Chem-Commun 1571
39. Wang L, Shi J, Yu J, Yan D (1998) Nanostruct Mater 10:1289